



OPEN ACCESS

EDITED BY

Esmeralda Mendoza-Mendoza,
Autonomous University of San Luis Potosí,
Mexico

REVIEWED BY

Ke Wu,
Beijing Technology and Business University,
China
Katharine Tibbetts,
Virginia Commonwealth University,
United States

*CORRESPONDENCE

R. Zanella,
✉ rodolfo.zanella@icat.unam.mx

RECEIVED 21 December 2023

ACCEPTED 20 February 2024

PUBLISHED 29 February 2024

CITATION

Camposeco R, Sánchez-Flores NA and
Zanella R (2024), Insights into CO oxidation on
Au/TiO₂-HMOR zeolite catalysts at
low temperature.
Front. Nanotechnol. 6:1359629.
doi: 10.3389/fnano.2024.1359629

COPYRIGHT

© 2024 Camposeco, Sánchez-Flores and
Zanella. This is an open-access article
distributed under the terms of the [Creative
Commons Attribution License \(CC BY\)](#). The use,
distribution or reproduction in other forums is
permitted, provided the original author(s) and
the copyright owner(s) are credited and that the
original publication in this journal is cited, in
accordance with accepted academic practice.
No use, distribution or reproduction is
permitted which does not comply with these
terms.

Insights into CO oxidation on Au/ TiO₂-HMOR zeolite catalysts at low temperature

R. Camposeco, N. A. Sánchez-Flores and R. Zanella*

Instituto De Ciencias Aplicadas y Tecnología, Universidad Nacional Autónoma De México, Mexico
City, Mexico

The effect of combining TiO₂ and mordenite zeolite (HMOR), employed as support of gold nanoparticles, on the CO oxidation reaction at low temperature is studied. The amount of TiO₂ encapsulated into HMOR was varied and the catalyst efficiency was investigated. The deposition-precipitation with urea (DPU) method was used to deposit gold nanoparticles; likewise, the synthesis of monometallic catalysts based on TiO₂ and HMOR is reported. The synthesized materials were characterized by X-ray diffraction (XRD), nitrogen adsorption, X-ray photoelectron spectroscopy (XPS), Fourier-transform infrared spectroscopy (FTIR), and transmission electron microscopy (TEM). The addition of TiO₂ influenced the properties of the TiO₂-HMOR composite, and its catalytic performance in the CO oxidation from 20°C. It was established that the 5Au/(28)TiO₂-HMOR composite was the most active catalyst at lower temperatures, which was ascribed to the close contact among the components of the TiO₂-HMOR composite, gold dispersion, gold and TiO₂ loadings, and Au and Ti species present in the catalysts.

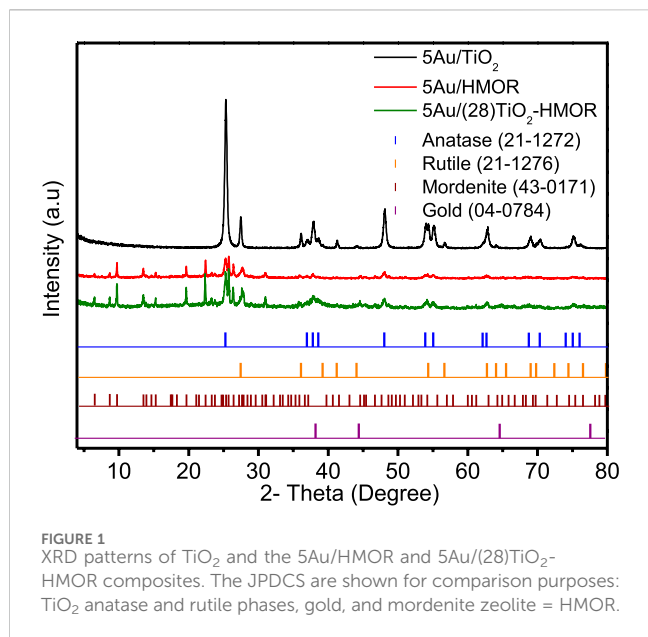
KEYWORDS

oxidation, dispersion, gold, zeolite, composite

1 Introduction

Zeolite is a porous aluminosilicate material with a characteristic three-dimensional structure that has been extensively employed as ion exchanger, adsorbent, and catalyst (Sircar et al., 2003; Farrusseng and Tuel, 2016). In the case of mordenite (HMOR), it is a zeolite that is used principally as a catalyst for different reactions such as hydrocracking, alkylation, and reforming (Vermeiren and Gilson, 2009; Vogt and Weckhuysen, 2015). On the other hand, gold nanoparticles have been deposited on zeolites, prepared as dealuminated or non-dealuminated mordenite, finding that the dealuminated support was responsible for the stability of Au¹⁺ species and its participation in the catalytic CO oxidation (Simakov et al., 2008). Likewise, gold nanoparticles supported on Y-type zeolite, pretreated with helium at 500°C, were found to be smaller and more uniformly distributed than those on Y-type zeolite without any surface pretreatment (Chen et al., 2005). Moreover, it has been shown that the modification of zeolites with different metal ions such as Fe, Ce and Ti (Tuzovskaya et al., 2007) leads to the improvement of their acidic properties and catalytic performance, as well as the stabilization of gold species (Lin et al., 2002).

Earlier studies have reported that the use of zeolites as carriers in TiO₂ synthesis provokes TiO₂ particle sizes that are smaller than the ones of bare TiO₂ (Fernandez-Catala et al., 2020), making the use of zeolites desirable for obtaining high dispersion of TiO₂ nanoparticles. In accordance with previous studies, the support for gold catalysts has a



significant effect on their performance, mainly for oxidation reactions (Chen et al., 2017). In this way, it has been informed that zeolites are an excellent matrix due to advantages such as high surface area and the ability to stabilize small gold particles within their small and well-size-controlled pores (Yan et al., 2004). Nevertheless, zeolite catalysts are thought of as inert supports, presenting poor catalytic activity when interacting with gold nanoparticles (Smolentseva et al., 2006), because they sinter easily when the Au/zeolite catalyst activation temperature increases. This happens because SiO₂ and related materials present a weak metal-support interaction with gold (Petcu et al., 2022). Recently, zeolites also began their path to be more efficient, for example, Ichikawa et al. incorporated Au(I) ions into the NaY zeolite by a solid-vapor reaction using Au₂Cl₆ (Mohamed et al., 2001); also, Au/HMordenite has been used as a catalyst in the oxidation of CO, showing activity between 50°C and 250°C (Tuzovskaya et al., 2007). In another way, the incorporation of cerium into the Au/Ce/Mordenite catalyst significantly increased the oxidation of CO, which reached 100%

conversion at 125°C (Qi et al., 2012). Likewise, manganese caused a similar effect on the Mn/Au/Mordenite catalyst, where the gold particles were smaller (2–15 nm) than those of a catalyst without manganese (7–50 nm) and most importantly, there was a considerable increase in the CO oxidation activity (Zamaro et al., 2015). However, there is a lack of information about the behavior of Au supported on the TiO₂-HMOR zeolite as a potential catalyst for the CO oxidation reaction.

Studies on TiO₂-zeolite composites have been mainly focused on photocatalysis applications (Hu et al., 2021), however, works employing these materials in catalytic thermal oxidation reactions have been more limited. In this work, a series of TiO₂-HMOR zeolite catalysts, in which the TiO₂ loading was varied (7, 21 and 28 wt%) and gold nanoparticles with the same loading (5 wt%) were incorporated, was employed to examine their catalytic properties in the CO oxidation. It is shown that these composites were active from 0°C and the characterization of the Au/TiO₂-HMOR zeolite catalysts revealed that the dispersion of gold and creation of Ti⁴⁺/Ti³⁺ and Au¹⁺/Au⁰ species are important factors to remarkably enhance their activity in the CO oxidation reaction.

2 Experimental

2.1 Preparation of the zeolite HMOR and TiO₂-HMOR samples

Mordenite CBV 20A with Si/Al of 20 in ammonia form (crystal diameter of 100–200 nm, purchased from Zeolyst International) was transformed into the acid form (HMOR) by calcination at 580°C for 3 h in air flow. Three samples of 1g of TiO₂-HMOR were prepared by incipient wetness impregnation, which were named as (7)TiO₂-HMOR, (21)TiO₂-HMOR and (28)TiO₂-HMOR according to the titanium oxide composition (7, 21 or 28 wt%).

Initially, TiO₂-Degussa P25 (47 m² g⁻¹, nonporous, 70% anatase and 30% rutile, purity >99.5%, purchased from Sigma-Aldrich) was dissolved in ethanol and mixed ultrasonically for 5 min. Then, the mixture was left and mixed with HMOR for 5 min in a porcelain crucible. After this action, the mixture was dried at 110°C overnight and calcined at 450°C for 6 h in air flow.

TABLE 1 Properties of the 2Au/TiO₂, 5Au/TiO₂, 5Au/HMOR, and 5Au/(28)TiO₂-HMOR composite catalysts treated at 300°C under H₂ atmosphere, and kinetic data during the CO oxidation reaction.

Property	2Au/TiO ₂	5Au/TiO ₂	5Au/HMOR	5Au/(28)TiO ₂ -HMOR
Nominal Au content, wt%	2	5	5	5
Actual Au content wt%	1.9	4.1	4.1	4.7
S _{BET} , m ² /g	46	47	445	313
Activation energy E _a , kJ/mol	32.8	33.8	62.5	36.7
Au particle size, nm	2.2	3.0	4.7	3.3
Au Dispersion, %	48	33	21	30
Rate, mol _{CO} /mol _{Au} •s (at 20°C)	0.0018	0.0025	0.0009	0.0022
TOF (s ⁻¹)	0.125	0.143	0.008	0.187

*Turnover frequency (TOF) calculated at room temperature under kinetic conditions using conversions below 20%.

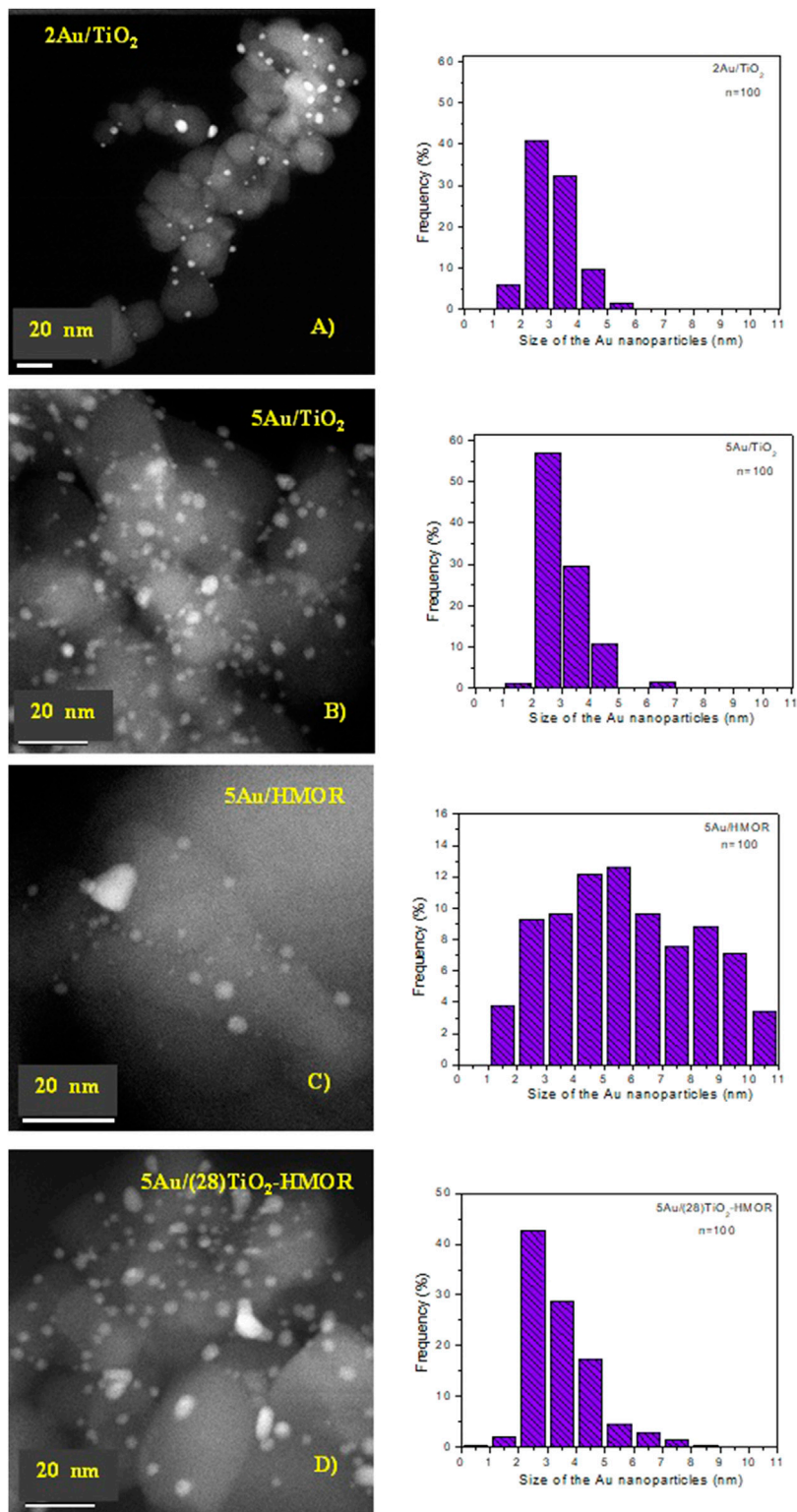
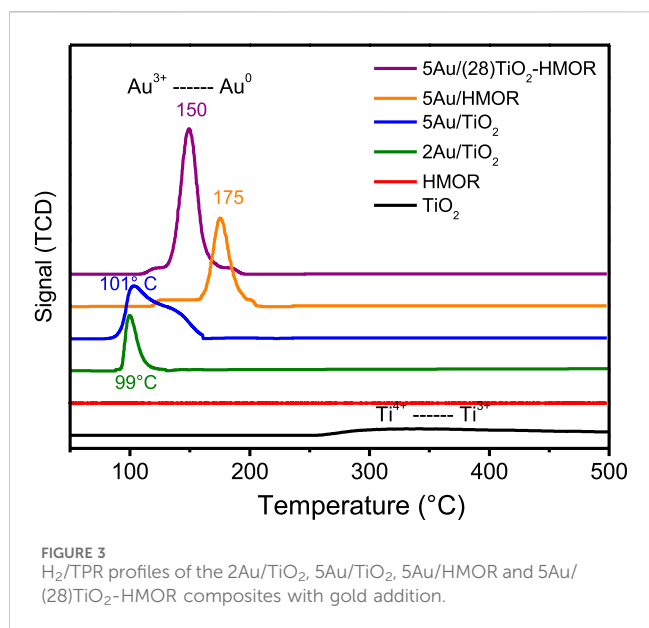


FIGURE 2 HRTEM/STEM images of the (A) 2Au/TiO₂, (B) 5Au/TiO₂, (C) 5Au/HMOR and (D) 5Au/(28)TiO₂-HMOR composites and their corresponding histograms by counting 100 particles thermally treated at 300°C under hydrogen atmosphere.



activated *in-situ* at a flow rate of 40 mL min⁻¹ of hydrogen or air, with a heating rate of 2°C min⁻¹ up to the final chosen temperature, between 250°C and 400°C, followed by a temperature plateau of 2 h. The feed gas mixture (1 vol% of CO and 1 vol% of O₂ balanced with N₂) was introduced with a total flow rate of 100 mL min⁻¹ and a heating rate of 2°C min⁻¹. The gases were analyzed with an online gas chromatograph (6890N, Agilent Technologies) equipped with a FID detector, HP Plot Q column and a methanizer. Stability tests of the catalysts *versus* time on stream were performed at 20°C during a continuous run of 24 h, employing 40 mg of catalyst activated *in-situ* in hydrogen at the same heating rate and temperature plateau as described above; likewise, in order to measure the reaction rates and activation energies, experimental conditions were determined so as to perform these measurements under kinetic regime. Consequently, the reaction rates and Arrhenius plots were determined with catalysts with a dilution of 50%, due to the high activity displayed by the catalysts. The turnover frequencies (TOF) of CO molecules converted per surface atom of gold particles and per second were determined from the reaction rates obtained under the kinetic regime and gold dispersion (surface atoms/total atoms in the particle).

2.2 Incorporation of gold into the TiO₂-HMOR samples

Gold (HAuCl₄·3H₂O 99.99% trace metals basis were purchased from Sigma-Aldrich) particles were obtained by the deposition-precipitation with urea (DPU) method. The gold concentration was 5 wt%. A sample containing 2 wt% of gold was also prepared on TiO₂ for comparison. For the preparation of the samples, 500 mg of 5Au/TiO₂, 5Au/HMOR, 5Au/(7)TiO₂-HMOR, 5Au/(21)TiO₂-HMOR and 5Au/(28)TiO₂-HMOR were added to this solution under constant stirring; thereafter, the suspension temperature was increased up to 80°C and stirring was kept constant for 16 h. After the DPU procedure, all the samples were centrifuged, washed with water at 50°C four times and then centrifuged and dried under vacuum for 2.5 h at 80°C.

2.3 Carbon monoxide oxidation test

In a flow reactor, the CO oxidation reaction was studied at atmospheric pressure, using 40 mg of dried catalyst that was first

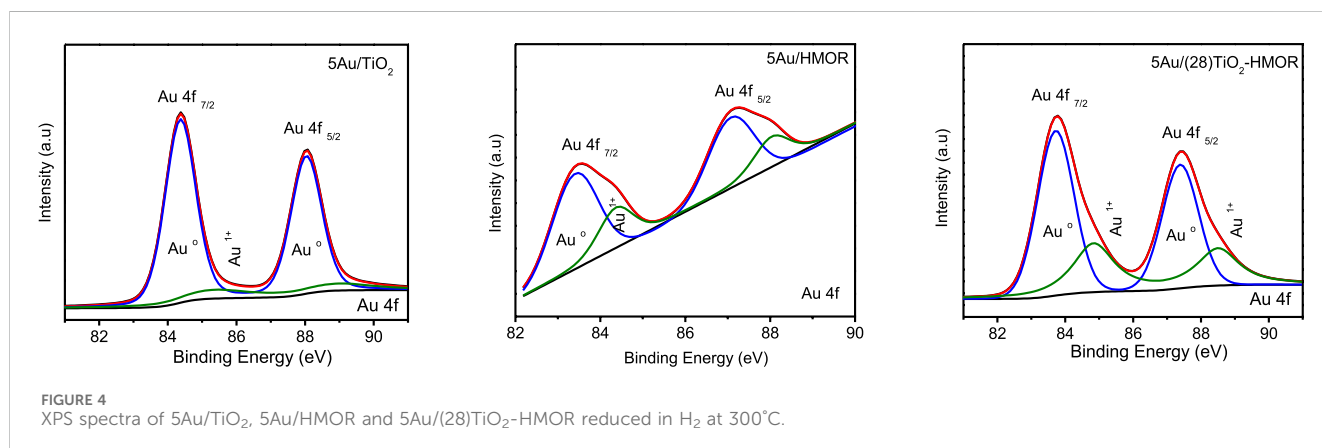
2.4 Characterization techniques

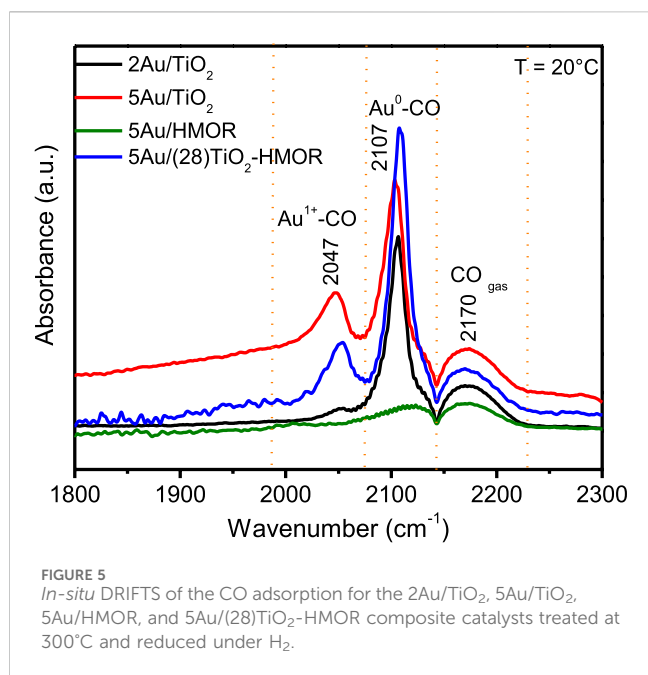
X-ray diffraction patterns were acquired at room temperature with Cu K α radiation in a Bruker Advance D-8 diffractometer having a theta-theta configuration and a graphite secondary-beam monochromator. The data were collected for scattering angles (2 θ) ranging from 4° to 80° with a step size of 0.01° for 2 s per point.

Images of the samples were obtained by HR-TEM analyses, employing a JEOL 2200FS microscope operating at 200 kV and equipped with a Schottky-type field emission gun and an ultrahigh resolution pole piece (Cs = 0.5 mm, point-to-point resolution, 0.190 nm). The textural properties were obtained by means of an ASAP-2000 analyzer from Micromeritics.

The specific surface area (SBET) was calculated from the Brunauer-Emmett-Teller (BET) equation from N₂ physisorption at 77 K. The pore size distribution was calculated by the Barrett-Joyner-Halenda (BJH) method from the desorption branch.

H₂-TPR profiles were produced on a Micromeritics AutoChem II chemisorption analyzer unit under flow of a 10% H₂/Ar gas





mixture (25 mL min⁻¹) with a heating rate of 10°C min⁻¹ from room temperature to 600°C.

DRIFTS results of *in-situ* CO oxidation were collected on an FTIR spectrometer (Nicolet iS50R FTIR) equipped with a Harrick DRIFT cell in the 400–4000 cm⁻¹ interval with 128 scans at a resolution of 4 cm⁻¹ using ZnSe windows. In a typical experiment, the powder samples were pretreated in air (40 mL min⁻¹) at 200°C for 2 h to remove the residuals. After cooling down to 20°C, a background spectrum was collected at 4-cm⁻¹ resolution for 128 scans in N₂ atmosphere.

3 Results

3.1 XRD results

The X-ray diffraction (XRD) patterns of the TiO₂, HMOR and TiO₂-HMOR composites with gold addition are plotted in Figure 1. According to earlier studies, 5Au/TiO₂ mainly revealed the feature peaks assigned to the anatase and rutile phases (Kim et al., 2021). Regarding the 5Au/(28)TiO₂-HMOR composite, it did not clearly show the diffraction peaks related to the presence of TiO₂, however, an increase in the intensity of the peak at 2 theta at 25.3° and 37.8° could reveal the presence of the TiO₂ anatase phase, see Figure 1. In this sense, the outcomes of the XRD patterns for 5Au/(28)TiO₂-HMOR indicate that the structural damage was insignificant during the ion-exchange process and that TiO₂ particles, occupying the mordenite cavities, were too small to be perceived by XRD, displaying negligible crystallite phases (anatase or rutile) like those observed in 5Au/TiO₂. The absence of peaks related to gold species was an evidence of good dispersion of Au in the 5Au/(28)TiO₂-HMOR material, see Figure 1. The surface areas of TiO₂ and the 5Au/HMOR and 5Au/(28)TiO₂-HMOR composites are given in Table 1. The measured surface area of TiO₂ (47 m²/g)

was notably lower than the ones of the 5Au/HMOR and 5Au/(28)TiO₂-HMOR catalysts, 445 and 313 m²/g, respectively. These results clearly revealed the presence of TiO₂ and gold inside the pores of HMOR zeolite, which showed a surface area of (560 m²/g). The decrease in the measured surface area of the catalysts could be due to a partial obstruction of HMOR pores by both the Au metal particles and TiO₂ crystals.

3.2 HRTEM/STEM morphology

Figure 2 shows HRTEM/STEM micrographs for the 5Au/HMOR and 5Au/(28)TiO₂-HMOR samples. It was feasible to quantify the size of the gold nanoparticles deposited in all the samples. For 5Au/TiO₂, the average gold diameter was ~3 nm, while the gold nanoparticles deposited on the mordenite zeolite showed an average diameter of ~4.7 nm, see Figures 2A, B, while the 5Au/(28)TiO₂-HMOR composite displayed nanoparticles close to ~3 nm in size, very similar to the one of the 5Au/TiO₂ sample, see Figure 3C. The 5Au/(28)TiO₂-HMOR composites revealed a good Au dispersion, indicating good interaction between gold and the TiO₂-HMOR composite, while 5Au/HMOR showed a poorer dispersion of gold because of the weak gold/mordenite surface interaction. In Supplementary Figure S1, HRTEM micrographs show that by using the deposition-precipitation with urea method, gold nanoparticles were deposited on the surface of TiO₂, HMOR and TiO₂-HMOR interface.

3.3 H₂/TPR

Figure 3 exhibits the H₂/TPR profile of the as-prepared materials dried under vacuum at 80°C. The H₂/TPR profiles of the 5Au/HMOR and 5Au/(28)TiO₂-HMOR materials displayed a well-resolved peak with maxima at ~175°C and ~150°C, respectively. In contrast, the 2Au/TiO₂ and 5Au/TiO₂ materials showed one wide peak with maximum at ~100°C, associated with gold reduction; these peaks can be assigned to the reduction of Au³⁺ species, deposited during the synthesis process, toward Au⁰, which is in agreement with previous studies (Zhang et al., 2018; Huang et al., 2022). A weak hydrogen consumption peak with maximum at ~350°C for the TiO₂-25 Evonik support could be assigned to the reduction of Ti⁴⁺ to Ti³⁺, according to Huang et al. (Huang et al., 2022); see also Supplementary Figure S2. Hence, the reduction peaks observed at 100, 150°C and 175°C could be linked to the successive reduction of Au³⁺ toward Au⁰ (Zhang et al., 2018). It is worth mentioning that the result of the TPR profiles of the materials with similar gold contents is different in the reduction temperature interval of gold species. These differences could be related to gold dispersion and TiO₂ content present in the mordenite zeolite materials, which may affect the temperature of gold reduction. It can be seen that the reduction of gold happened within the interval between 90°C and 220°C.

3.4 XPS

Figure 4 shows the XPS spectra of the 5Au/TiO₂, 5Au/HMOR and 5Au/(28)TiO₂-HMOR samples. The deconvolution shows four peaks assigned to Au⁰ (Au4f_{7/2} and Au4f_{5/2} situated at 83.5 and 87.5 eV, severally) and to Au¹⁺ (Au4f_{7/2} and Au4f_{5/2} detected at 85.0 and 88.5 eV, respectively) (Sahoo and Ke, 2021). The main difference is observed in the presence and quantity of Au¹⁺, where

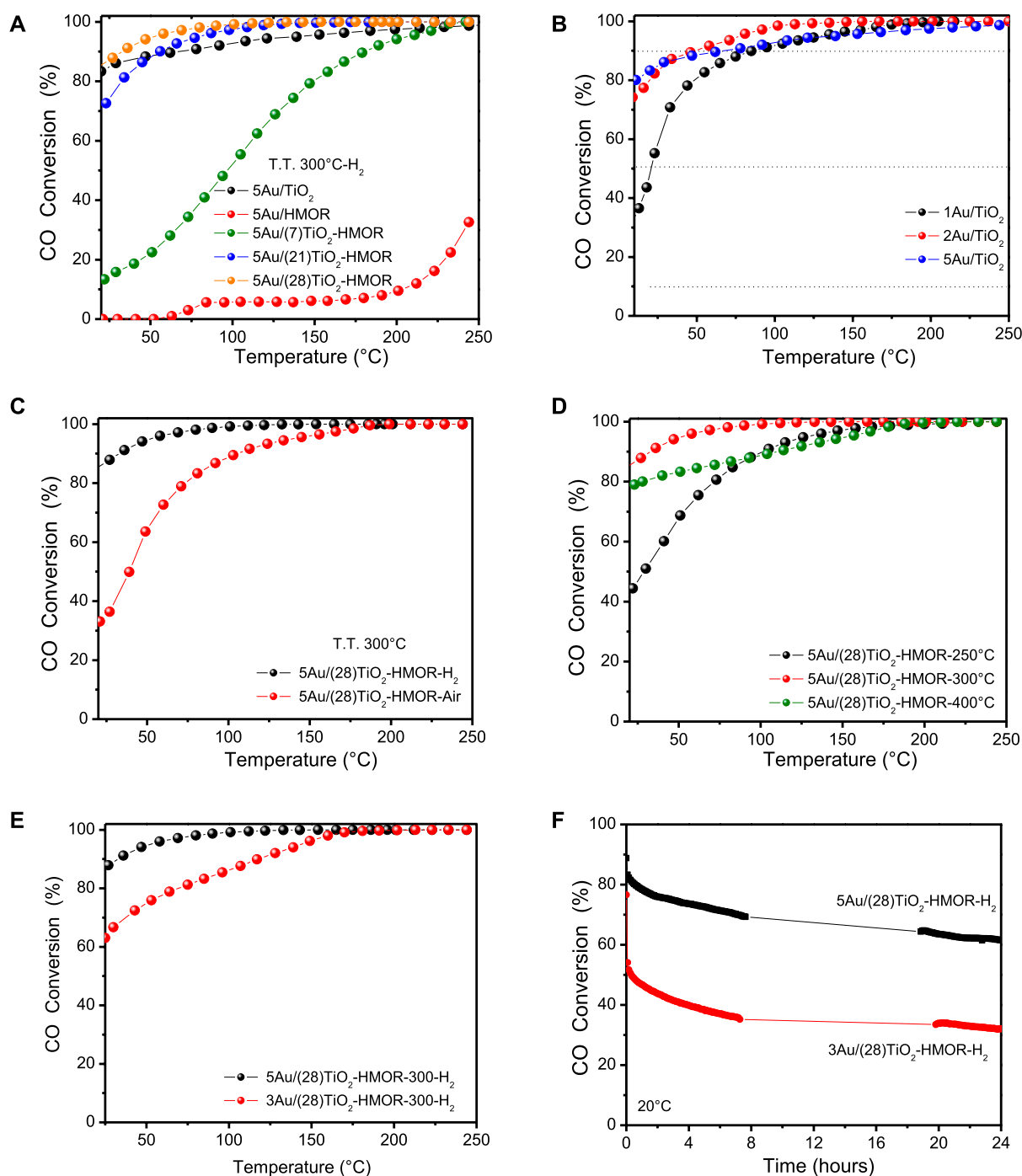


FIGURE 6

Temperature profiles and performance displayed by the tested catalysts: (A) 5Au/TiO₂, 5Au/HMOR and 5Au/(28)TiO₂-HMOR; (B) Temperature profiles and performance displayed by the Au/TiO₂ catalysts with different loads; (C) comparison of CO conversions as functions of the reaction temperature for the 5Au/(28)TiO₂-HMOR catalysts with different atmospheres; (D) comparison of CO conversions for the 5Au/(28)TiO₂-HMOR catalysts with different temperatures; (E) effect of gold loadings (3 and 5 wt%) for samples thermally treated in hydrogen flow at 300°C; and (F) temporal stability for 24 h for 3Au/(28)TiO₂-HMOR and 5Au/(28)TiO₂-HMOR at 20°C under dry conditions.

the peak corresponding to this species was less intense than the one for the 5Au/TiO₂ material, followed by the 5Au/HMOR and 5Au/(28)TiO₂-HMOR samples, respectively. The peaks related to Au⁰ were more noticeable than the peaks earmarked to ionic gold, evidencing the transition from Au³⁺ to Au⁰ by the thermal

treatment under hydrogen atmosphere. Thus, it is suggested that the presence of Au¹⁺ may be related to the stronger interaction between gold particles and TiO₂ as well as to the TiO₂ and HMOR support when the sample was thermally treated under hydrogen atmosphere. According to the deconvolution results, the percentages

TABLE 2 Comparison chart of reaction temperatures for the CO oxidation reaction using gold-mordenite catalysts.

Catalyst	Temperature [°C]	Au loading (wt%)	Ref
Au-Cu/Mordenite	100–300	1.9–2.7	Petcu et al. (2022)
Au-Ce/Mordenite	50–175	3.0	Zamaro et al. (2015)
Au-Mn/Mordenite	50–350	0.6–1.1	Hu et al. (2021)
5Au/(28)TiO ₂ -HMOR	<20–150	3.0–5.0	This work

of gold species in the catalysts were: for 5Au/TiO₂, Au⁰ (87%) and Au¹⁺ (13%); for 5Au/HMOR, Au⁰ (72%) and Au¹⁺ (28%); and for 5Au/(28)TiO₂-HMOR, Au⁰ (64%) and Au¹⁺ (36%). However, as the intensity of the 4f gold peaks is different, the dominant presence of metallic gold (Au⁰) was observed in all the samples. The results evidenced the significance of Au¹⁺ in the CO oxidation reaction at low temperature (see Table 1 and CO oxidation results below). In this line, the interaction between gold nanoparticles and the TiO₂, HMOR and TiO₂-HMOR supports is totally different. Gold nanoparticles supported on TiO₂, TiO₂-HMOR and HMOR revealed the existence of Au⁰ and Au¹⁺ species, the latter at lower proportion. Moreover, shifts in the position of the peaks corresponding to the metallic gold species of 0.2 eV, between TiO₂ and TiO₂-HMOR, and of 0.8 eV with regard to HMOR were observed, evidencing that a strong interaction between Au and TiO₂ took place, which meant electron transfer between the Au particles and TiO₂-HMOR support, mainly observed with the incorporation of 28 wt% of TiO₂ and 5 wt% of gold.

3.5 CO adsorption followed by DRIFTS

Figure 5 shows the comparison of the CO-DRIFT spectra after 30 min of CO exposure at room temperature for the 5Au/TiO₂, 5Au/HMOR, and 5Au/(28)TiO₂-HMOR composite catalysts reduced *in-situ* under H₂ at 300°C. The band at 2175 cm⁻¹, whose intensity is very similar in all the catalysts, is associated with the presence of CO in gas phase. For 5Au/TiO₂, the occurrence of a single carbonyl band at 2107 cm⁻¹ associated with linear CO adsorbed on low coordinated surface Au⁰ atoms was observed (Atwi et al., 2020). The 5Au/HMOR sample does not present bands ascribed to CO adsorption. In the case of the 5Au/(28)TiO₂-HMOR composite, the band at 2107 cm⁻¹, related to CO adsorbed on Au⁰, was noted. An additional contribution at 2047 cm⁻¹ is observed in the 5Au/TiO₂ and 5Au/(28)TiO₂-HMOR composites, which is associated with CO adsorption by distinct gold species, denoting the appearance of Au¹⁺-CO, Au^{δ-}-CO, and Au³⁺-CO species (Feyzbar-Khalkhali-Nejad et al., 2021). In the case of 5Au/HMOR, these adsorption signals were not evident, demonstrating that the quantity of bridging CO species on Au is null. Moreover, the strength of the bands of CO linearly adsorbed on Au⁰ is more intense in 5Au/TiO₂ and 5Au/(28)TiO₂-HMOR than the one observed in 5Au/HMOR, Figure 5. These results also suggest the existence of an interaction between metallic Au and TiO₂ in the 2Au/TiO₂, 5Au/TiO₂ and 5Au/(28)TiO₂-HMOR catalysts. In summary, when the 2Au/TiO₂, 5Au/TiO₂, 5Au/HMOR, and 5Au/(28)TiO₂-HMOR composite catalysts were reduced *in-situ* under H₂ at 300°C, gold was

reduced forming Au⁰-CO as well as Au¹⁺-CO as shown in Figure 5. These results suggest that Au had an interaction that induced a modification in the adsorption properties of the 2Au/TiO₂, 5Au/TiO₂, and 5Au/(28)TiO₂-HMOR catalyst surfaces, resulting in more active surfaces at low temperature, thus influencing the performance of the catalysts, as shown in the next section.

3.6 Catalytic activity in the CO oxidation reaction

The carbon monoxide oxidation activity as a function of the reaction temperature for the 5Au/TiO₂, 5Au/HMOR and 5Au/(28)TiO₂-HMOR samples under dry reaction conditions was evaluated, and the test results are depicted in Figure 6A. It is observed that the temperature for complete conversion of CO for the 5Au/(28)TiO₂-HMOR sample was lower than the ones for the 5Au/(21)TiO₂-HMOR and 5Au/(7)TiO₂-HMOR samples, suggesting that the presence of TiO₂ and Au nanoparticles promoted significantly the CO oxidation from 0°C, mainly when the TiO₂ actual content was 28 wt%, which showed complete CO conversion at 70°C. It is noticed that the CO catalytic activity decreased when the TiO₂ content reached 7 and 21 wt%, which was possibly due to the fact that part of the active sites was not in interaction with TiO₂ in HMOR. The 5Au-TiO₂ catalyst displayed much higher catalytic activity than 5Au/HMOR (Table 1). The incorporation of 5 wt% of gold into TiO₂ enhanced the CO oxidation at 50°C (87% of conversion), whereas 5Au/HMOR showed poorer performance, only 38% of conversion was reached at 250°C; likewise, 5Au/(28)TiO₂-HMOR improved the CO oxidation at 50°C (94% of conversion) with regard to 5Au/HMOR and 5Au/TiO₂. As a comparison, the T₉₀ values were 87, 94% and 92% of conversion for the Au/TiO₂ catalyst for 1, 2, and 5 wt% of Au loading, respectively, see Figure 6B, suggesting that the addition of a higher gold loading on TiO₂ did not have a great impact on the conversion at low temperature, as it occurred with the TiO₂/HMOR composite, see Figure 6E. Also, it is interesting to note that the 5Au/(28)TiO₂-HMOR catalyst thermally treated at 300°C in H₂ was more active than the one thermally treated in air at 300°C.

Afterwards, the most active catalyst composition, 5Au/(28)TiO₂-HMOR, was chosen to further investigate different parameters such as temperature, gas treatment and stability, as shown in Figure 6 C, D and E. The thermal treatment in the activation of a catalyst is a variable that also affects its performance. The CO oxidation outcomes for 5Au/(28)TiO₂-HMOR activated at different temperatures under hydrogen atmosphere are shown in Figure 5B. First, the 5Au/(28)TiO₂-

HMOR sample treated at 300°C was the one that showed the highest initial conversion and the one that reached 100% CO oxidation at lower temperature (100°C). Then, the catalyst that was activated with H₂ at 400°C, presented activity that was lower than that of the 5Au/(28)TiO₂-HMOR sample at 300°C whose initial CO conversion was 79% at 20°C. On the other hand, the same catalyst treated at 250°C had much lower initial activity and showed 44.4% of conversion at 20°C.

Therefore, the catalysts activated at 400°C and 250°C not only lowered their activity at room temperature, but also required higher temperature to reach 100% of conversion. In Figure 6C, it is observed that 100% of CO conversion was reached at reaction temperatures near 200°C; therefore, a thermal treatment at 300°C in H₂ produced the most active 5Au/(28)TiO₂-HMOR catalysts. Otherwise, since the best activation temperature was 300°C, this temperature was used to thermally treat the same sample under air flow, however, that sample showed lower initial CO conversion (33.1%), and reached 100% of CO conversion at 200°C, which is similar to the performance of the 5Au/(28)TiO₂-HMOR catalyst activated at 300°C in hydrogen flow, Figure 6D. In this sense, in earlier studies about the synthesis of gold catalysts, Au³⁺ species were identified after drying the sample; therefore, the thermal treatment using either H₂ or air atmosphere reduced Au³⁺ toward Au⁰ (Qwabe et al., 2019), and it has been shown that even during a thermal treatment under air, the gold precursor decomposes with temperature to form Au⁰ due to the instability of Au₂O₃ (Bond, 2001). On the other hand, previous studies have mentioned that thermal treatment under H₂ has resulted in smaller gold particles than those obtained under air, because H₂ leads to stronger interaction between the gold particles and TiO₂ support and prevents particle sintering (TsubotaCunningham et al., 1995).

Figure 6E shows the light-off CO oxidation curves for 5Au/(28)TiO₂-HMOR thermally treated at 300°C under hydrogen atmosphere, varying the gold loading from 3 to 5 wt%. The CO conversion of 5Au/(28)TiO₂-HMOR was 89% at 20°C, showing a T₉₀ value of 27°C; the 3Au/(28)TiO₂-HMOR catalyst displayed 62% of CO conversion at 20°C, and a T₉₀ value of 125°C; then, the gold loading had a significant impact on the TiO₂-HMOR sample behavior. In fact, gold particles loaded on oxides that have been tested in the oxidation of CO have demonstrated that the catalytic activity is influenced by both the annealing temperature and gold loading (Haruta et al., 1993). Moreover, Figure 6F presents the stability at 20°C for the 3Au/(28)TiO₂-HMOR and 5Au/(28)TiO₂-HMOR catalyst thermally treated under hydrogen atmosphere at 300°C. Slight deactivation occurred during the first 24 h and then, the CO conversion remained almost stable mainly for the 5Au/(28)TiO₂-HMOR catalyst.

The behavior of the 5Au/(28)TiO₂-HMOR catalyst in the CO oxidation was compared with other catalysts reported in the literature, see Table 2. According to the results obtained in this study in terms of characterization and catalytic activity for CO oxidation at low temperature, the most promising outlook seems to indicate that the incorporation of TiO₂ into HMOR exerts an important effect on the final properties of the composite. The Au/HMOR zeolite itself presents poor performance in the oxidation of CO; likewise, the combination of TiO₂ and zeolite showed

interesting properties, such as small and more homogenous metal gold size and a suitable porous structure, allowing improved catalytic activity of the 5Au/(28)TiO₂-HMOR composite with regard to 5Au/-HMOR; due to these reasons, the 5Au/(28)TiO₂-HMOR composite is an efficient alternative for CO oxidation at low temperature compared with similar catalysts reported in the literature using the zeolite mordenite as support, see Table 2.

4 Conclusion

Mordenite zeolite as a support of gold nanoparticles is not suitable as a catalytic material in the oxidation of CO. However, the incorporation of TiO₂ into mordenite and the deposition of gold nanoparticles allow the synthesis of efficient catalytic materials for the CO oxidation process at low temperatures. Hence, the addition of TiO₂ to mordenite promotes the partial covering of the structural channels of the zeolite. Additionally, it was possible to observe increasing efficiency at room temperature (20°C) in the CO oxidation, mainly in terms of the turnover frequency as the TiO₂ content in the mordenite zeolite grew up to 28 wt%, considering that the pure TiO₂ support showed efficiency of 97% at room temperature and which indicates that a support prepared with 28% TiO₂ displayed very close efficiency. This fact enabled the assertion that the intrinsic porosity of the zeolite allowed better diffusion of CO through the catalyst and that the gold nanoparticles were more exposed due to the surface area of the composite because of the structural channels, high gold dispersion, TiO₂ and HMOR interaction and presence of Au¹⁺ species that allowed CO oxidation at low temperatures.

Data availability statement

The original contributions presented in the study are included in the article/Supplementary Material, further inquiries can be directed to the corresponding author.

Author contributions

RC: Writing—original draft, Writing—review and editing, Investigation. NS-F: Writing—original draft, Writing—review and editing, Funding acquisition, Methodology. RZ: Funding acquisition, Writing—original draft, Writing—review and editing, Conceptualization, Supervision.

Funding

The author(s) declare financial support was received for the research, authorship, and/or publication of this article. Consejo Nacional de Humanidades Ciencias y Tecnologías (CONACYT) through the CB A1-S-18269 grant and Direccion General de Asuntos del Personal Academico-UNAM through the PAPIIT IN104022 grant.

Acknowledgments

The authors want to thank the financial support provided by the Consejo Nacional de Humanidades Ciencias y Tecnologías (CONAHCYT) through the CB A1-S-18269 grant, Dirección General de Asuntos del Personal Académico-UNAM through the PAPIIT IN104022 grant. RC gratefully acknowledges CONAHCYT for the postdoctoral scholarship. We thank the technical support provided by Viridiana Maturano.

Conflict of interest

The authors declare that the research was conducted in the absence of any commercial or financial relationships that could be construed as a potential conflict of interest.

References

- Atwi, R., Elgayyar, T., Cadete Santos Aires, F. J., Tuel, A., and Meunier, F. C. (2020). RETRACTED ARTICLE: revisiting the evolution of IR spectra of CO adsorbed on Au nanoparticles supported on non-reducible supports. *Top. Catal.* 63, 1596–1605. doi:10.1007/s11244-020-01372-2
- Bond, G. C. (2001). Gold: a relatively new catalyst. *Gold Bull.* 34, 117–119. doi:10.1007/bf03214823
- Chen, J. H., Lin, J. N., Kang, Y. M., Yu, W. Y., Kuo, C. N., and Wan, B. Z. (2005). Preparation of nano-gold in zeolites for CO oxidation: effects of structures and number of ion exchange sites of zeolites. *Appl. Catal. A General* 291, 162–169. doi:10.1016/j.apcata.2005.02.038
- Chen, Y.-H., Mou, C.-Y., and Wan, B.-Z. (2017). Ultrasmall gold nanoparticles confined in zeolite Y: preparation and activity in CO oxidation. *Appl. Catal. B Environ.* 218, 506–514. doi:10.1016/j.apcatb.2017.06.083
- Farrusseng, D., and Tuel, A. (2016). Perspectives on zeolite-encapsulated metal nanoparticles and their applications in catalysis. *New J. Chem.* 40, 3933–3949. doi:10.1039/c5nj02608c
- Fernandez-Catala, J., Sanchez-Rubio, M., Navlani-Garcia, M., Berenguer-Murcia, A., and Cazorla-Amorós, D. (2020). Synthesis of TiO₂/nanozeolite composites for highly efficient photocatalytic oxidation of propene in the gas phase. *ACS omega* 5 (48), 31323–31331. doi:10.1021/acsomega.0c04793
- Feyzbar-Khalkhali-Nejad, F., Hassani, E., Rashti, A., and Oh, T. S. (2021). Adsorption-based CO removal: principles and materials. *J. Environ. Chem. Eng.* 9 (4), 105317. doi:10.1016/j.jece.2021.105317
- Haruta, M., Tsubota, S., Kobayashi, T., Kageyama, H., Genet, M. J., and Delmon, B. (1993). Low-temperature oxidation of CO over gold supported on TiO₂, α-Fe₂O₃, and Co₃O₄. *J. Catal.* 144 (1), 175–192. doi:10.1006/jcat.1993.1322
- Hu, G., Yang, J., Duan, X., Farnood, R., Yang, C., Yang, J., et al. (2021). Recent developments and challenges in zeolite-based composite photocatalysts for environmental applications. *Chem. Eng. J.* 417, 129209. doi:10.1016/j.cej.2021.129209
- Huang, W., Zhou, Y., Wei, Q., Liu, X., Zhang, P., Xu, Z., et al. (2022). Synthesis of mesoporous TiO₂-Al₂O₃ composites supported NiW hydrotreating catalysts and their superior catalytic performance for heavy oil hydrodenitrogenation. *Fuel* 319, 123802. doi:10.1016/j.fuel.2022.123802
- Kim, M. G., Kang, J. M., Lee, J. E., Kim, K. S., Kim, K. H., Cho, M., et al. (2021). Effects of calcination temperature on the phase composition, photocatalytic degradation, and virucidal activities of TiO₂ nanoparticles. *ACS omega* 6 (16), 10668–10678. doi:10.1021/acsomega.1c00043
- Lin, J. N., Chen, J. H., Hsiao, C. Y., Kang, Y. M., and Wan, B. Z. (2002). Gold supported on surface acidity modified Y-type and iron/Y-type zeolite for CO oxidation. *Appl. Catal. B Environ.* 36, 19–29. doi:10.1016/s0926-3373(01)00276-4
- Mohamed, M. M., Salama, T. M., Ohnishi, R., and Ichikawa, M. (2001). Characterization of gold (I) in dealuminated H-mordenite zeolite. *Langmuir* 17 (18), 5678–5684. doi:10.1021/la001403f
- Petcu, G., Anghel, E. M., Buixaderas, E., Atkinson, I., Somacescu, S., Baran, A., et al. (2022). Au/Ti synergistically modified supports based on SiO₂ with different pore geometries and architectures. *Catalysts* 12 (10), 1129. doi:10.3390/catal12101129
- Qi, L., Tang, C., Zhang, L., Yao, X., Cao, Y., Liu, L., et al. (2012). Influence of cerium modification methods on catalytic performance of Au/mordenite catalysts in CO oxidation. *Appl. Catal. B Environ.* 127, 234–245. doi:10.1016/j.apcatb.2012.08.013
- Qwabe, L. Q., Friedrich, H. B., and Singh, S. (2019). Remediation of CO by oxidation over Au nanoparticles supported on mixed metal oxides. *J. Environ. Chem. Eng.* 7 (1), 102827. doi:10.1016/j.jece.2018.102827
- Sahoo, S. R., and Ke, S. C. (2021). Spin-orbit coupling effects in Au 4f core-level electronic structures in supported low-dimensional gold nanoparticles. *Nanomaterials* 11 (2), 554. doi:10.3390/nano11020554
- Simakov, A., Tuzovskaya, I., Bogdanchikova, N., Pestryakov, A., Avalos, M., Farias, M. H., et al. (2008). Influence of sodium on activation of gold species in Y-zeolites. *Catal. Commun.* 9, 1277–1281. doi:10.1016/j.catcom.2007.11.027
- Sircar, S., and Myers, A. L. (2003). “Gas separation by zeolites,” in *Handbook of zeolite science and Technology*. Editors S. M. Auerbach, K. A. Carrado, and P. K. Dutta (New York: Marcel Dekker Inc.), 1063–1104.
- Smolentseva, E., Bogdanchikova, N., Simakov, A., Pestryakov, A., Tuzovskaya, I., Avalos, M., et al. (2006). Influence of copper modifying additive on state of gold in zeolites. *Surf. Sci.* 600, 4256–4259. doi:10.1016/j.susc.2006.01.153
- TsubotaCunningham, S. D. A. H., Bando, Y., and Haruta, A. M. (1995). Preparation of nanometer gold strongly interacted with TiO₂ and the structure sensitivity in low-temperature oxidation of CO. *Stud. Surf. Sci. Catal.* 91, 227–235. doi:10.1016/s0167-2991(06)81759-3
- Tuzovskaya, I. V., Simakov, A. V., Pestryakov, A. N., Bogdanchikova, N. E., Gurin, V. V., Farias, M. H., et al. (2007). Co-existence of various active gold species in Au-mordenite catalyst for CO oxidation. *Catal. Commun.* 8 (7), 977–980. doi:10.1016/j.catcom.2006.10.014
- Vermeiren, W., and Gilson, J. P. (2009). Impact of zeolites on the petroleum and petrochemical industry. *Top. Catal.* 52, 1131–1161. doi:10.1007/s11244-009-9271-8
- Vogt, E. T. C., and Weckhuysen, B. M. (2015). Fluid catalytic cracking: recent developments on the grand old lady of zeolite catalysis. *Chem. Soc. Rev.* 44, 7342–7370. doi:10.1039/c5cs00376h
- Yan, W., Chen, B., Mahurin, S., Hagaman, E., Dai, S., and Overbury, S. H. (2004). Surface sol-gel modification of mesoporous silica materials with TiO₂ for the assembly of ultrasmall gold nanoparticles. *J. Phys. Chem. B* 108, 2793–2796. doi:10.1021/jp037713z
- Zamaro, J. M., Boix, A. B., and Martínez-Hernández, A. (2015). CO oxidation over Au supported on Mn-ZSM5 and Mn-MOR. *Catal. Commun.* 69, 212–216. doi:10.1016/j.catcom.2015.06.018
- Zhang, A., Zhang, L., Jing, G., Zhang, H., Wang, S., Su, H., et al. (2018). Promotion of Au³⁺ reduction on catalytic performance over the Au/CuO/CeO₂ catalysts for preferential CO oxidation. *Int. J. Hydrogen Energy* 43 (22), 10322–10333. doi:10.1016/j.ijhydene.2018.04.081

Publisher's note

All claims expressed in this article are solely those of the authors and do not necessarily represent those of their affiliated organizations, or those of the publisher, the editors and the reviewers. Any product that may be evaluated in this article, or claim that may be made by its manufacturer, is not guaranteed or endorsed by the publisher.

Supplementary material

The Supplementary Material for this article can be found online at: <https://www.frontiersin.org/articles/10.3389/fnano.2024.1359629/full#supplementary-material>